Ultrasensitive detection of norovirus using a magnetofluoroimmunoassay based on synergic properties of gold/magnetic nanoparticle hybrid nanocomposites and quantum dots

Ultrasensitive detection of norovirus using a magnetofluoroimmunoassay based on synergic properties of gold/magnetic nanoparticle hybrid nanocomposites and quantum dots

Kenshin Takemura[a], Jaewook Lee[b,¶], Tetsuro Suzuki[c], Thoshimi Hara[d], Fuyuki Abe[d], Enoch Y. Park[a,b,*]

[a] Laboratory of Biotechnology, Department of Bioscience, Graduate School of Science and Technology, Shizuoka University, 836 Ohya, Suruga-ku, Shizuoka 422-8529, and [b]Research Institute of Green Science and Technology, Shizuoka University, 836 Ohya, Suruga-ku, Shizuoka 422-8529, Japan

[c]Department of Infectious Diseases, Hamamatsu University School of Medicine, 1-20-1 Higashi-ku, Handa-yama, Hamamatsu 431-3192, Japan

[d]Department of Microbiology, Shizuoka Institute of Environment and Hygiene, 4-27-2, Kita-ando, Aoi-ku, Shizuoka 420-8637, Japan

E-mail addresses:
takemura.kenshin.16@shizuoka.ac.jp (KT)
nanojaewook@outlook.com (JL)
tesuzuki@hama-med.ac.jp (TS)
toshimi1_hara@pref.shizuoka.lg.jp (TH)
fuyuki1_abe@pref.shizuoka.lg.jp (FA)
park.enoch@shizuoka.ac.jp (EYP)

[¶]Current affiliation: School of Materials Science, Japan Advanced Institute of Science and Technology, Asahidai 1-1, Nomishi, Ishikawa 923-1292, Japan
[*] Corresponding author.
E-mail address: park.enoch@shizuoka.ac.jp (E. Y. Park)

ABSTRACT

Norovirus is the cause of the contagious disease gastroenteritis, and the infection is easy to spread because of the high infectivity of this virus. When the virus infects elderly people and young children, it may progress to severe disease. To prevent this hygienic threat, the development of highly sensitive and rapid detection methods is urgently needed. In this study, we developed a localized surface plasmon resonance (LSPR)-amplified magnetofluoroimmunoassay that can be used to detect norovirus even in biocomplex media without decreasing the fluorescence response. A multi-functional gold nanoparticle (AuNP) and magnetic nanoparticle (MNP) hybrid nanocomposite was synthesized. The AuNP/MNP hybrid nanocomposites and CdSeS quantum dots (QDs) were conjugated by the anti-norovirus genogroup II antibody (Ab). This hybrid nanocomposite made it possible to separate the target virus from impurities by a magnetic field and induced a high LSPR effect. Target virus was added to the Ab-conjugated AuNP/MNP composite and Ab-CdSeS QDs, and then Au/MNPs-Ab-virus-Ab-CdSeS QDs were separated by using an external magnetic field. The target norovirus-like particles can be detected in the range of 1 pg/ml to 5 ng/ml with a limit of detection (LOD) of 0.48 pg/ml in feces. This detection method was applied to clinical samples of feces containing norovirus from patients, and the LOD was 84 copies of RNA/ml without being affected by the impurities contained in the feces solution. This novel sensing system is suitable for norovirus detection in feces samples and for on-site detection.

Keywords: AuNP/MNP hybrid nanocomposite, Localized surface plasmon resonance, Magnetic separation of virus, Magnetofluoroimmunoassay, Norovirus

1. Introduction

Recently, hybrid nanomaterials have contributed to the development of biosensing platforms because of their excellent synergic properties, such as magneto-optical, magnetoplasmonic, and magnetocatalytic properties [1–5]. Ultimately, such hybrid nanostructures have been useful in the fabrication of highly sensitive and specific biosensing systems to overcome public concerns regarding infectious diseases [6]. Among several hybrid structures, plasmonic nanoparticle and magnetic nanoparticle (MNP) hybrid nanomaterials have been highlighted due to their multiple functionalities. The localized surface plasmon resonance (LSPR) of the plasmonic nanoparticles is an important and useful property because it can enhance or quench the fluorescence of quantum dots (QDs) through LSPR energy transfer between plasmonic nanoparticles and QDs [7-9]. The fluorescence intensity can be tuned depending on the distance between the plasmonic nanoparticles and the QDs. It was reported regarding the distance factor that the fluorescence was enhanced by an approximately 10–15 nm gap and quenched within a 5 nm gap [10]. Through this interaction, a highly sensitive and selective optical sensing system has been developed to detect viruses, DNA and other biomolecules [11–14]. The MNP showed excellent potential for bioapplication in various fields [15–17]. In particular, because the movement of MNP can be controlled by an external magnetic field, target biomaterials can be easily separated from the impurities contained in a solution [18–20]. Through this approach, a target virus in a mixture with impurities can be isolated and detected [21]. In addition, the plasmonic and magnetic synergy properties of AuNP/MNP nanohybrid composites have been utilized for various applications [22, 23].

Norovirus (NoV) is one of the major causes of the infectious disease gastroenteritis and is transmitted from food, water, the environment or another person. Symptoms of the infection include nausea and serious stomachache, vomiting, headache, diarrhea and chills

[24]. Genetically, the NoV is divided into six gene groups (GI to GVI), and furthermore, according to recent studies, these gene groups are subdivided into 38 gene clusters [25]. The gene groups show differences in terms of the infection route [26], infectivity, and ability to bind to receptors. Distinct genotypic differences are reported, particularly between foodborne infection and human-to-human transmission [26]. The GII type constitutes a high proportion of virus infection among humans and foodborne infection, especially GII.4 [27]. In epidemic gastroenteritis caused by NoV occurring within the United States from September 2009 to August 2013, 72% of the total disease was caused by GII.4 [28]. The GII NoV are most important because of the most infected people are confirmed compare with other genogroups, which urgently requires a simple on-site detection method.

In this study, NoV was detected by using a confetto-AuNP/MNP nanohybrid composite and QDs via an LSPR-amplified magnetofluoroimmunoassay (MFIA). The magnetoplasmonic substrate-based confetto-AuNP/MNP nanohybrid composite is involved in two key processes: target virus separation with an external magnetic field and LSPR-based plasmonic resonance energy transfer. The QDs served as signal transducers to monitor the target virus. This hybrid sensing system showed high sensitivity and selectivity, and, even when the target virus was mixed with human feces, there was no loss of sensitivity.

2. Materials and methods

2.1. Materials and instruments

HEPES buffer, sorbitan monolaurate (Tween 20), polyoxyethylene (20), sulfuric acid sodium acetate, hydrogen peroxide, acetone, chloroform, potassium hydroxide (KOH) and methanol were purchased from Wako Pure Chemical Ind. Ltd. (Osaka, Japan). Oleic acid

was purchased from Nacalai Tesque Inc. (Kyoto, Japan). Bovine serum albumin (BSA), HAuCl□, mercaptoundecanoic acid (11-MUA), *N*-hydroxysuccinimide (NHS), and *N*-(3-dimethylaminopropyl)-*N'*-ethylcarbodiimide hydrochloride (EDC) were purchased from Sigma-Aldrich (St Louis, USA).

UV/vis absorption and fluorescence emission measurements were performed using a filter-based multimode microplate reader (Infinite F200M; TECAN, Ltd, Männedorf, Switzerland). Transmission electron microscopy (TEM; JEM-2100F, JEOL, Ltd., Tokyo, Japan) and scanning TEM for energy dispersive X-ray spectrometry (EDS) were used for morphological observation of nanoparticles under operation conditions of 100 kV and 200 kV, respectively. The zeta potential and hydrodynamic particle size were measured by dynamic light scattering (DLS) using a Zetasizer Nano series (Malvern Inst. Ltd., Malvern, UK). The magnetic properties of the AuNP/MNP composites were determined using a superconducting quantum interference device (SQUID; MPMS-7, Quantum Design, Inc., San Diego, USA). Fourier transform infrared spectroscopy was performed using FT/IR-6600 (JASCO, Tokyo, Japan). Powder X-ray diffraction (PXRD) analysis was carried out using a RINT ULTIMA XRD (Rigaku Co., Tokyo, Japan) with a Ni filter and a Cu-Kα source. Data were collected over 2theta = 30–90º at a scan rate of 0.01º/step and 10 s/point.

2.2. Biological materials and fecal sample preparation

Goat anti-rabbit IgG-HRP was purchased from Santa Cruz Biotechnology. Influenza virus A/California/07/2009 (H1N1) and influenza virus A/Netherlands/219/03 (H9N2) were purchased from Vircell Microbiologists (Granada, Spain) and Prospec-Tany TechnoGene Ltd. (Rehovot, Israel), respectively. An anti-NoV antibody broadly reactive to genogroup II (Monoclonal antibody NS14) was used in this work [29, 30]. NS14 was derived from spleen cells of mice immunized orally and the isotype was IgG. This antibody

purified by protein G and the concentration is 0.3 mg/ml. G Ⅱ.4 NoV-like particles (NoV-LPs) were expressed in *Trichoplusia ni*, BTL-Tn 5B1-4 (Tn5) (Invitrogen, San Diego, CA, USA) by transfection of recombinant baculovirus TCN-VP1 [31]. Expressed NoV-LPs was purified and quantified according to the standard method of virus-like particle preparation. Clinically isolated NoVs (G Ⅱ 2. 3. 4.) were collected from 100 mg of fecal samples of patients with infectious gastroenteritis, including foodborne illness, as determined by inspections based on laws and ordinances. Each clinical sample was defined of concentration by real time RT-PCR. A commercial NoV detection kit (NV-AD III) was purchased from Denka Seiken Co., Ltd. Tokyo, Japan, for comparison. NoV sampling was performed according to the guidelines of the Ethics Committee of the Environment and Hygiene Institute in Shizuoka Prefecture (September 14, 2016).

2.3. Synthesis of a confetto-AuNP/MNP nanocomposite

A AuNP/MNP nanohybrid composite was synthesized in two steps at room temperature. Superparamagnetic iron oxide nanoparticles (SPIONs) were synthesized and functionalized by surface modification as described in a previous study [32]; briefly, the MNPs were synthesized based on the coprecipitation of ferric and ferrous ion solutions. Ten milliliters of ammonium hydroxide were added to ferric chloride (5 mmol) and ferrous chloride (10 mmol) in 40 ml of deionized (DI) water. After rapid stirring for 30 min at room temperature, the MNPs were purified by magnetic separation, followed by washing three times with ethanol. The MNPs were dispersed in 36 ml of water, and then, 21.6 mM tetrachloroauric(III) acid ($HAuCl_4$) was added to the MNP solution. The Au^{3+} ions were physically adsorbed on the MNPs and converted to AuNPs using 0.1 M HEPES buffer as a reducing agent [33] during 30 min of stirring at 40°C. Unabsorbed AuNPs were removed by magnetic separation. To functionalize the AuNP/MNP nanocomposite with antibody,

11-MUA was used to coat the surface of AuNP/MNP: 1 mg/ml AuNP/MNP was mixed with 0.1 M 11-MUA in a pH 2 solution under nitrogen gas in an oxygen-free environment. The 11-MUA-capped AuNP/MNP nanocomposite was purified by magnetic separation and washed three times using ultrapure water.

2.4. Conjugation of antibody

The carboxylic group on the nanoparticles formed chemical bonds with anti-NoV antibody (NS14 Ab) via carbodiimide EDC/NHS coupling [34]. L-Glutathione (GSH)-capped CdSeS core QDs were synthesized and characterized according to our previous protocol [11]. The carboxyl group of 11-MUA on the AuNP/MNP nanocomposite and QDs was activated by EDC and NHS. The activated carboxyl group was conjugated with NS14 Ab through an amide bond; first, 1 ml of 11-MUA/AuNP/MNP and 1 ml of QDs were mixed with 500 µl of 0.1 M EDC and stirred for 30 min at room temperature individually, after which 500 µl of 0.1 M NHS and 5.1 µg of NS14 Ab were added to the mixture and stirred over 16 h at 7°C.The Ab-conjugated AuNP/MNP nanocomposite was separated magnetically and washed three times using 1 ml of deionized (DI) water. The Ab-conjugated QDs were purified by centrifugation at 6500 × g for 5 min at 7°C and redissolved in DI water. Finally, the purified nanomaterials were dissolved in 5 ml of DI water. The magnetic nanoparticles (1 ml) used for the detection sensitivity comparison experiment with the AuNP/MNP were conjugated with 5.1 µg of NS14 by electrostatic conjugation using the charge on the surface of MNP by mixing with the antibody for 30 minutes at room temperature.

2.5. Magnetofluoroimmunoassay (MFIA) for detection of NoV-LPs and NoV

Ab-AuNP/MNP nanocomposites and Ab-QDs were mixed at a ratio of 1:3 in a 1.5 ml

plastic tube. Upon adding 20 µl of NoV-LPs or NoV solution to this mixture, an immune response occurred after 5 min at room temperature. The NoV induced formation of a sandwich hybrid structure through virus and antibody interaction, which was a QD-Ab-NoV-Ab-AuNP/MNP nanocomposite. This sandwich hybrid structure was separated magnetically within 3 min and redissolved in DI water, and then fluorescence was measured. In addition, NoV-LPs in human feces were detected by AuNP/MNP-based MFIA to compare the detection performance and sensing behavior with the case without impurity. In this case, the detection performance was evaluated with 1 pg/ml to 10 ng/ml NoV-LPs in feces.

NoV was isolated from clinical feces samples collected from infected patients. A 100 mg quantity of fecal sample was suspended in 900 µL of phosphate-buffered saline (PBS, pH 7.4); after separation of the solids, the supernatant was used as the detection sample. The concentration of these samples were determined by real-time RT-PCR (G Ⅱ.2: 6.2×10□ RNA copy/ml, G Ⅱ.3: 7.2×10^8 RNA copy/ml, G Ⅱ.4: 5.7×10□ RNA copy/ml). In this case, the detection performance was evaluated in ranging from 100 RNA copy/ml to 10□ RNA copy/ml NoV in feces sample. The detection assay was excited at 400 nm, and the fluorescence detection was carried out in the range of 410–700 nm. The fluorescence peak of CdSeS QDs was observed at 610 nm. Fluorescence enhancement was defined as the ratio (F/F_0) of the fluorescence intensity value (F) of sample and that of the control (F□). The clinically isolated NoVs for which quantification was determined by real-time RT-PCR were also assayed using a commercial NoV detection kit (NV-AD III) for comparison with our proposed method.

2.6. Detection of the biosensor

AuNP/MNP nanocomposites have two functions of simple rapid separation of the

target virus from an impurity-containing solution and signal amplification of LSPR between the AuNP/MNP nanocomposite and QDs on the target viruses. The target viruses were captured by Ab-AuNP/MNP nanocomposites and Ab-QDs to form Ab-AuNP/MNP, virus and Ab-QD sandwich structures. Then, QD-Ab-virus-Ab-Au/MNPs were separated by using an external magnetic field, and the separated nanocomplexes were resuspended in ultrapure water. Here, the fluorescence intensity of QDs was enhanced by LSPR energy transfer from AuNPs to QDs, as shown in Scheme 1. The fluorescence enhancement is dependent on the concentration of the target virus.

<< Scheme 1>>

3. Results and discussion

3.1. Characterization of AuNP/MNP nanohybrid composites

The morphology and size of MNPs and AuNP/MNPs were observed by TEM (Fig. 1A–D). The MNPs were round in shape, with a size between 10 nm and 20 nm. The AuNP/MNP nanohybrid structure formed a round shape with a size of 10 nm (Fig. 1B) and a confetto shape on the surface of the MNPs with a size of 40 nm (Fig. 1C, D). Au ions were attached on the surface of the MNPs by electrostatic interactions and were reduced to AuNPs by HEPES buffer and heat. The formation and growth of AuNPs is closely related to the reaction temperature [35]. In addition, the reduction potential of the reducing agent is also a considerable factor because certain reductants could control not only the growth rate but also the shape of the AuNPs [36]. The size and shape of the AuNPs was also affected by two factors: reaction temperature (40°C and 80°C) and HEPES buffer as a reducing agent. The Au ions were physically adsorbed on the surface of the MNPs through electrostatic interactions at room temperature for 30 min with shaking. Then,

HEPES buffer was added to the mixture, and the reaction temperature was increased to 40°C with stirring for 30 min. During the reaction, the Au ions were converted to AuNPs on the MNPs, and interestingly, confetto-shaped AuNPs were formed. The presence of HEPES buffer can induce the random growth of AuNPs, which is attributed to the confetto shape. However, at 80°C with HEPES buffer, AuNPs were spherical. This meant that the temperature was a key factor for the preparation of confetto-shaped AuNPs, and it was believed that the reactivity of HEPES buffer was changed at 80°C. When the temperature was raised, the reduction rate was extremely fast due to thermal energy, so the time to grain formation was decreased, and small round nanoparticles were formed because the random growth of the surface was not induced. As a result, the surface structure and size difference were affected by different thermal conditions.

On the other hand, elemental analysis of the confetto-shaped AuNP/MNP structure was carried out by using STEM (Fig. S1A–C). Au and Fe were clearly observed. The peaks of Au overlapped with those of Fe, suggesting that Au existed on the Fe base structure. Additionally, the element peaks of Au (La 9.712, M 2.120) and Fe (La 6.398, M 0.705) were measured from the EDS spectrum (Fig. S1D). Additionally, PXRD analysis clearly showed the formation of AuNPs on the MNPs by the presence of specific 2θ peaks of AuNPs at 38.2°, 44.3°, 64.4°, 77.6°, and 81.8°, which indicated the lattice pattern (111), (200), (220), (311), and (222) after forming the composite (Fig. S2). This result also proves that AuNPs are attached on the MNPs.

The plasmonic absorbance of the AuNP/MNP hybrid structures was analyzed depending on the reaction temperature and the spectra, as shown in Fig. 1E. According to the absorbance spectra, the λ_{max} of the plasmonic absorbance band of confetto-shaped AuNPs was approximately 632 nm. In addition, the secondary plasmonic absorbance band was slightly observed at approximately 750 nm, and this band was correlated with the

plasmonic coupling interaction between closely located confetto-shaped AuNPs on the SPIONs [1, 37–39]. According to the TEM image of confetto-shaped AuNPs on the SPIONs, several AuNPs contacted each other on the surface of SPIONs, suggesting that the result of plasmonic coupling absorbance coincided with the TEM image. On the other hand, the plasmonic absorbance of spherical AuNPs synthesized at 100□ in 4 ml of 0.1 M HEPES buffer was measured at approximately 558 nm. The absorbance spectrum peak of spherical AuNPs has already been reported [40]. The AuNPs with a size of 14.8 nm showed an absorbance peak at 517 nm, and those with sizes of 48.3 nm showed a peak at 533 nm. According to the TEM image of the spherical AuNP/MNP, the average diameter was 10 to 20 nm even though the particles were not uniform. The absorbance spectra did not correspond to the same size of AuNPs because the particles formed composites. Additionally, the confetto-shaped AuNP/MNP nanocomposite had a clearly different spectral peak than the spherical AuNPs of the same size. This SPR band was also proof of the confetto-shaped AuNP/MNP because this band was attributed to their surface structure [41]. After modification of the 11-MUA on the surface of AuNPs by an EDC/NHS-based Ab coupling reaction, the plasmonic absorbance showed similar absorbance spectra at each temperature (Fig. 1E, dashed spectra). This meant that the LSPR property of AuNP/MNPs was not changed after 11-MUA modification.

<<Figure 1>>

The magnetic properties of Au/MNP were characterized by SQUID, and these properties were important for the magnetic separation process. The magnetic-hysteresis loops of MNP and AuNP/MNP are shown in Fig. 1F and G, and these were obtained at room temperature because the magnetic separation process was carried out at room

temperature. The coercive force of the MNP was 8 Oe and – 8 Oe, and the remanence effect was indicated at approximately 0.04 emu/g and – 0.04 emu/g. After AuNP modification on the surface of the MNPs, the coercive force of the hybrid nanomaterial was measured at approximately 2 Oe and – 2 Oe, and the remanence effect was approximately 0.03 emu/g and – 0.03 emu/g. Thus, after preparation of the hybrid nanomaterial, the magnetic property was maintained.

3.2. Conjugation of antibody onto the AuNP/MNP nanocomposites

The ratio of Ab conjugation on the surface of the hybrid nanomaterial depends on the size of the AuNPs on the MNPs. In particular, the confetto-shaped AuNPs have a stronger LSPR area at the particle edge than do normal spherical-shaped AuNPs. This means that energy transfer from confetto-shaped AuNPs to QDs for fluorescence enhancement occurred more efficiently than that from spherical AuNPs [42, 43]. The conditions for Ab conjugation with AuNPs were optimized depending on the morphology of the AuNPs on MNPs. After the EDC/NHS coupling reaction between the Ab and AuNPs, Ab binding on the AuNPs was confirmed by ELISA according to a previously described protocol (Supporting Information S3 and Fig. S3). According to Fig. 2A, all AuNP/MNP composites were conjugated by antibodies. The thiol group of 11-MUA has high affinity for gold and carboxyl groups, which resulted in chemical conjugation with amino groups of antibodies than MNPs. This result showed that AuNP/MNP composites were functionalized by 11-MUA.

To compare the sensing ability depending on the difference in the shape and structure of the AuNPs on the MNPs, an LSPR-based fluoroimmunoassay was carried out with 10 pg/ml NoV-LPs. The confetto-shaped AuNP/MNPs at room temperature and 40°C showed strong fluorescence enhancement after adding the target virus, and confetto-shaped AuNPs

(80°C) led to an enhanced response compared with the spherical AuNP/MNP composites (Fig. 2B). The confetto-shaped AuNP/MNP composites were shown to be potential LSPR-amplified nanomaterials.

<<Figure 2>>

3.3. LSPR-amplified MFIA of NoV-LPs by minimizing the effect of impurities in the clinical sample

Based on the preliminary study, NoV-LP was detected by using Ab-conjugated confetto-shaped AuNP/MNPs and CdSeS QDs through magnetic separation in the LSPR-amplified MFIA. The Ab-conjugation on each nanomaterial was confirmed via ELISA, and high absorbance was shown for the Ab-AuNP/MNP nanocomposite and Ab-CdSeS QD cases, as shown in Fig. S3. The anti-NS14 antibody also showed strong binding with the NoV-LPs (Fig. S4).

Based on this detection strategy, the NoV-LPs in the DI water and feces were detected, and their fluorescence intensities are shown in Fig. 3. With increasing concentrations of NoV-LPs, the fluorescence intensity of QD also gradually increased, and this phenomenon was observed not only in DI water but also in the fecal samples (Fig. 3A). Interestingly, a similar sensitivity was shown in both samples, and the linearity of the calibration curve was also almost the same in both cases (Fig. 3B). This means that the NoV-LPs were successfully separated from the impurities contained in feces by using Au/MNP nanocomposites and an external magnetic field; consequently, NoV-LPs in a complex biomedium can be detected without interference by impurities. Excellent sensitivity in both cases was exhibited. The limit of detection (LOD) was calculated by multiplying the standard deviation (δ) of 10 separate measurements (n=10) by 3 and dividing by the slope

(K) of the linear calibration curve (LOD=3δ/K). The LOD was calculated to be 0.24 pg/ml in DI water and 0.48 pg/ml in feces from calculation (δ=24.2) Furthermore, the visualization of diagnosis was carried out after the magnetic separation process by using confocal laser scanning microscopy (Fig. 3C–D). The fluorescence of magnetically separated QD-(NoV-LP)-AuNP/MNPs was clearly observed; thus, target NoV-LPs were visually observed via this detection method.

<<Figure 3>>

On the other hand, the detection performance of this sensing system was also compared to that without magnetic separation (Ab-AuNP and Ab-QD) and without LSPR (Ab-MNP and Ab-QD) (Figs. S5 and S6). LSPR fluorescence enhancement was observed in ultrapure water, but it was significantly decreased in the feces sample solution (Fig. S5). This result showed that magnetic separation is useful for applying the LSPR-amplified MFIA to detect NoV from feces samples. When MNP and QD were used to detect NoV-LPs in ultrapure water, the fluorescence intensity was enhanced depending on the virus concentration, but the signal gap was low compared with the LSPR-immunofluorescence effect (Fig. S6) because there was no LSPR effect.

Several types of clinical NoVs (GII. 2, GII. 3, GII.4) from infected human feces were detected by using this sensing system (Fig. 4A). In GII.2 and GII.3 cases, the fluorescence of QDs linearly increased with the concentration of NoV (10^2 to 10□ RNA copies/ml), and the LOD was calculated to be 98 RNA copies/ml for GII. 2 and 84 RNA copies/ml for GII.3. However, the GII.4 showed low correlation coefficient compared two others, and the LOD was 934 copies/ml.

<<Figure 4>>

LSPR-amplified MFIA was compared with a commercial ELISA kit using clinical NoVs (GII. 2, GII. 3 and GII.4) (Fig. 4B). The chemiluminescence intensity increased from 10^4-10^5 RNA copies/ml of NoV, and this will be useful for detection of a large range of NoV. From this result, it was proven that this detection system has a sensitivity of approximately 100 times that of a commercially available ELISA kit. Recently Bioluminescent enzyme immunoassay (BLEIA) based on luminescent was developed for NoV detection from feces [44,45]. This detection method already automated (120 samples/h) and the LOD was estimated to be 0.25 pg/ml for NoV-LPs in PBS and 10^5 to 10^6 copies/g stool for clinically isolated NoV. This method showed almost similar LOD for NoV-LPs with MFIA, but the MFIA showed significatively improved detection performance for clinically isolated NoV in feces. In this work, we separated the target virus from feces, which improved detection performance without deterioration of fluorescence intensity. Moreover, it was shown that the sensitivity of this method was inferior when compared with the other sensitive detection system using other viral RNAs and structural protein, but it maintained sufficient sensitivity as a biosensor capable of detecting virus particles (Table 1). Therefore, this MFIA can be applied for on-site detection for real clinical samples because the target virus could be separated from impurities via a magnetic separation process without pretreatment.

<<Table 1>>

3.4. Selectivity of the LSPR-amplified MFIA.

The selectivity of the LSPR-amplified MFIA was investigated in the presence of

negative viruses such as influenza virus A(H7N7), influenza virus A(H9N2), hepatitis E virus-like particle, and zika virus. None of the tested negative controls increased the fluorescence intensity (Fig. 5). Thus, the results provide a strong indication that the LSPR-amplified MFIA is specific for NoV-LPs.

<<Figure 5>>

4. Conclusions

LSPR-amplified MFIA is demonstrated to be a highly sensitive, selective and facile detection method for NoV. The sensitivity of NoV-LPs was 0.24 pg/ml in DI water and 0.48 pg/ml in feces. Compared with that of a commercially available ELISA kit, the sensitivity of this detection method was approximately 1000 times higher. When this assay was applied to detect clinical samples, the LOD was 98 RNA copies/ml for GII. 2 and 84 RNA copies/ml for GII.3. Even though the sensitivity was different for different genotypes, this detection system stably detected NoV even in impurity-containing feces specimens. This detection method is suitable for on-site detection of NoV because of its excellent sensitivity and selectivity, with minimal effects due to impurities contained in clinical samples.

Conflict of interests

The authors declare no competing financial interest.

Acknowledgements

This research was supported by the Japan Society for the Promotion of Science (JSPS) Postdoctoral Fellowship for Overseas Researchers (16F16361). This work was supported in part by the Bilateral Joint Research Project of the JSPS, Japan.

Appendix A. Supplementary data

Supplementary material related to this article can be found, in the online version, at doi:https://doi: .

References

[1] J. Lee, K. Takemura, E.Y. Park, Plasmonic/magnetic graphene-based magnetofluoro-immunosensing platform for virus detection, Sensor. Actuat. B-Chem., 276 (2018) 254–261.

[2] D. Mortazavi, A.Z. Kouzani, A. Kaynak, W. Duan, Nano-plasmonic biosensors: A review, Complex Medical Engineering (CME), 2011 IEEE/ICME International Conference on, IEEE, 2011, pp. 31–36.

[3] J. Lee, M. Morita, K. Takemura, E.Y. Park, A multi-functional gold/iron-oxide nanoparticle-CNT hybrid nanomaterial as virus DNA sensing platform, Biosens. Bioelectron., 102 (2018) 425–431.

[4] J. Li, J.Z. Zhang, Optical properties and applications of hybrid semiconductor nanomaterials, Coord. Chem. Rev., 253 (2009) 3015–3041.

[5] J. Lee, K. Takemura, C.N. Kato, T. Suzuki, E.Y. Park, Binary Nanoparticle Graphene Hybrid Structure-Based Highly Sensitive Biosensing Platform for Norovirus-Like Particle Detection, ACS applied materials & interfaces, 9 (2017) 27298–27304.

[6] J. Lee, O. Adegoke, E.Y. Park, High‐Performance Biosensing Systems Based on Various Nanomaterials as Signal Transducers, Biotechnol. J., 14, (2018) 197005.

[7] K.M. Mayer, J.H. Hafner, Localized surface plasmon resonance sensors, Chem. Rev., 111 (2011) 3828–3857.

[8] K.A. Willets, R.P. Van Duyne, Localized surface plasmon resonance spectroscopy and sensing, Annu. Rev. Phys. Chem., 58 (2007) 267–297.

[9] J. Lee, J. Kim, S.R. Ahmed, H. Zhou, J.-M. Kim, J. Lee, Plasmon-induced

photoluminescence immunoassay for tuberculosis monitoring using gold nanoparticles decorated graphene, ACS applied materials & interfaces, 6 (2014) 21380–21388.

[10] S. Link, M.A. El-Sayed, Size and temperature dependence of the plasmon absorption of colloidal gold nanoparticles, The Journal of Physical Chemistry B, 103 (1999) 4212–4217.

[11] O. Adegoke, M. Morita, T. Kato, M. Ito, T. Suzuki, E.Y. Park, Localized surface p lasmon resonance-mediated fluorescence signals in plasmonic nanoparticle-quantum dot hybrids for ultrasensitive Zika virus RNA detection via hairpin hybridization assays, Biosens. Bioelectron., 94 (2017) 513–522.

[12] Q. Zhang, L. Wu, J.Z. Ten It Wong, X. Liu, X. Zhou, P. Bai, B. Liedberg, Y. Wang, Surface plasmon-enhanced fluorescence on Au nanohole array for prostate-specific antigen detection, International journal of nanomedicine, 12 (2017) 2307.

[13] J. Lee, S.R. Ahmed, S. Oh, J. Kim, T. Suzuki, K. Parmar, S.S. Park, J. Lee, E.Y. Park, A plasmon-assisted fluoro-immunoassay using gold nanoparticle-decorated carbon nanotubes for monitoring the influenza virus, Biosens. Bioelectron., 64 (2015) 311–317.

[14] K. Takemura, O. Adegoke, N. Takahashi, T. Kato, T.-C. Li, N. Kitamoto, T. Tanaka, T. Suzuki, E.Y. Park, Versatility of a localized surface plasmon resonance-based gold nanoparticle-alloyed quantum dot nanobiosensor for immunofluorescence detection of viruses, Biosens. Bioelectron., 89 (2017) 998–1005.

[15] P. Zou, Y. Yu, Y.A. Wang, Y. Zhong, A. Welton, C. Galbán, S. Wang, D. Sun, Superparamagnetic iron oxide nanotheranostics for targeted cancer cell imaging and pH-dependent intracellular drug release, Mol. Pharm., 7 (2010) 1974–1984.

[16] O. Veiseh, J.W. Gunn, M. Zhang, Design and fabrication of magnetic nanoparticles for targeted drug delivery and imaging, Adv. Drug Del. Rev., 62 (2010) 284–304.

[17] J. Jang, H. Lim, Characterization and analytical application of surface modified magnetic nanoparticles, Microchem. J., 94 (2010) 148–158.

[18] B. Samanta, H. Yan, N.O. Fischer, J. Shi, D.J. Jerry, V.M. Rotello, Protein-passivated Fe 3 O 4 nanoparticles: low toxicity and rapid heating for thermal therapy, J. Mater. Chem., 18 (2008) 1204–1208.

[19] I.S. Lee, N. Lee, J. Park, B.H. Kim, Y.-W. Yi, T. Kim, T.K. Kim, I.H. Lee, S.R. Paik, T. Hyeon, Ni/NiO core/shell nanoparticles for selective binding and magnetic separation of histidine-tagged proteins, J. Am. Chem. Soc., 128 (2006) 10658–10659.

[20] S. Bucak, D.A. Jones, P.E. Laibinis, T.A. Hatton, Protein separations using colloidal

magnetic nanoparticles, Biotechnol. Prog., 19 (2003) 477–484.

[21] H. Gu, K. Xu, C. Xu, B. Xu, Biofunctional magnetic nanoparticles for protein separation and pathogen detection, ChCom, (2006) 941–949.

[22] H. Zeng, S. Sun, Syntheses, properties, and potential applications of multicomponent magnetic nanoparticles, Advanced Functional Materials, 18 (2008) 391–400.

[23] N.C. Bigall, W.J. Parak, D. Dorfs, Fluorescent, magnetic and plasmonic—Hybrid multifunctional colloidal nano objects, Nano Today, 7 (2012) 282–296.

[24] F. Mattner, D. Sohr, A. Heim, P. Gastmeier, H. Vennema, M. Koopmans, Risk groups for clinical complications of norovirus infections: an outbreak investigation, Clin. Microbiol. Infect., 12 (2006) 69–74.

[25] L. Verhoef, J. Hewitt, L. Barclay, S. Ahmed, R. Lake, A.J. Hall, B. Lopman, A. Kroneman, H. Vennema, Norovirus Genotype Profiles Associated with Foodborne Transmission, 1999 ?" 2012, Emerg. Infect. Dis., 21 (2015) 592.

[26] L. Verhoef, H. Vennema, W. Van Pelt, D. Lees, H. Boshuizen, K. Henshilwood, M. Koopmans, F.-B.V.i.E. Network, Use of norovirus genotype profiles to differentiate origins of foodborne outbreaks, Emerg. Infect. Dis., 16 (2010) 617.

[27] M. Noda, S. Fukuda, O. Nishio, Statistical analysis of attack rate in norovirus foodborne outbreaks, Int. J. Food Microbiol., 122 (2008) 216–220.

[28] E. Vega, L. Barclay, N. Gregoricus, S.H. Shirley, D. Lee, J. Vinjé, Genotypic and epidemiologic trends of norovirus outbreaks in the United States, 2009 to 2013, J. Clin. Microbiol., 52 (2014) 147–155.

[29] B. Kou, S.E. Crawford, N.J. Ajami, R. Czakó, F.H. Neill, T.N. Tanaka, N. Kitamoto, T.G. Palzkill, M.K. Estes, R.L. Atmar, Characterization of cross-reactive norovirus-specific monoclonal antibodies, Clin. Vaccine Immunol., 22 (2015) 160–167.

[30] N. Kitamoto, T. Tanaka, K. Natori, N. Takeda, S. Nakata, X. Jiang, M.K. Estes, Cross-reactivity among several recombinant calicivirus virus-like particles (VLPs) with monoclonal antibodies obtained from mice immunized orally with one type of VLP, J. Clin. Microbiol., 40 (2002) 2459–2465.

[31] S.R. Ahmed, K. Takemeura, T.-C. Li, N. Kitamoto, T. Tanaka, T. Suzuki, E.Y. Park, Size-controlled preparation of peroxidase-like graphene-gold nanoparticle hybrids for the visible detection of norovirus-like particles, Biosens. Bioelectron., 87 (2017) 558–565.

[32] S.C. Hong, J.H. Lee, J. Lee, H.Y. Kim, J.Y. Park, J. Cho, J. Lee, D.-W. Han, Subtle cytotoxicity and genotoxicity differences in superparamagnetic iron oxide

nanoparticles coated with various functional groups, International journal of nanomedicine, 6 (2011) 3219.

[33] R. Chen, J. Wu, H. Li, G. Cheng, Z. Lu, C.-M. Che, Fabrication of gold nanoparticles with different morphologies in HEPES buffer, Rare Metals, 29 (2010) 180–186.

[34] M.J. Fischer, Amine coupling through EDC/NHS: a practical approach, Surface plasmon resonance, Springer2010, pp. 55–73.

[35] Y. Sun, Y. Xia, Shape-controlled synthesis of gold and silver nanoparticles, Sci, 298 (2002) 2176–2179.

[36] J. Xie, J.Y. Lee, D.I. Wang, Seedless, surfactantless, high-yield synthesis of branched gold nanocrystals in HEPES buffer solution, Chem. Mater., 19 (2007) 2823–2830.

[37] J. Lee, S. Mulmi, V. Thangadurai, S.S. Park, Magnetically aligned iron oxide/gold nanoparticle-decorated carbon nanotube hybrid structure as a humidity sensor, ACS applied materials & interfaces, 7 (2015) 15506–15513.

[38] J. Lee, J. Lee, Magneto-optically active magnetoplasmonic graphene, Chem. Comm., 53 (2017) 5814–5817.

[39] J. Lee, H. Zhou, J. Lee, Small molecule induced self-assembly of Au nanoparticles, J. Mater. Chem., 21 (2011) 16935–16942.

[40] W. Haiss, N.T. Thanh, J. Aveyard, D.G. Fernig, Determination of size and concentration of gold nanoparticles from UV− Vis spectra, Anal. Chem., 79 (2007) 4215–4221.

[41] P.K. Jain, K.S. Lee, I.H. El-Sayed, M.A. El-Sayed, Calculated absorption and scattering properties of gold nanoparticles of different size, shape, and composition: applications in biological imaging and biomedicine, The journal of physical chemistry B, 110 (2006) 7238–7248.

[42] C.L. Nehl, J.H. Hafner, Shape-dependent plasmon resonances of gold nanoparticles, J. Mater. Chem., 18 (2008) 2415–2419.

[43] D.E. Mustafa, T. Yang, Z. Xuan, S. Chen, H. Tu, A. Zhang, Surface plasmon coupling effect of gold nanoparticles with different shape and size on conventional surface plasmon resonance signal, Plasmonics, 5 (2010) 221–231.

[44] N. Shigemoto, Y. Tanizawa, T. Matsuo, N. Sakamaki, Y. Ohiro, S. Takayasu, S. Fukuda, Clinical evaluation of a bioluminescent enzyme immunoassay for detecting norovirus in fecal specimens from patients with acute gastroenteritis, J. Med. Virol., 86 (2014) 1219–1225.

[45] N. Sakamaki, Y. Ohiro, M. Ito, M. Makinodan, T. Ohta, W. Suzuki, S. Takayasu, H. Tsuge, Bioluminescent enzyme immunoassay for the detection of norovirus capsid antigen, Clin. Vaccine Immunol., 19 (2012) 1949–1954.

[46] R. Chand, S. Neethirajan, Microfluidic platform integrated with graphene-gold nano-composite aptasensor for one-step detection of norovirus, Biosens. Bioelectron., 98 (2017) 47–53.

[47] Z. Han, Q. Weng, C. Lin, J. Yi, J. Kang, Development of CdSe–ZnO Flower-Rod Core-Shell Structure Based Photoelectrochemical Biosensor for Detection of Norovirous RNA, Sensors, 18 (2018) 2980.

[48] B.S. Batule, S.U. Kim, H. Mun, C. Choi, W.-B. Shim, M.-G. Kim, Colorimetric Detection of Norovirus in Oyster Samples through DNAzyme as a Signaling Probe, J. Agric. Food Chem., 66 (2018) 3003–3008.

[49] A.A. Trujillo, K.A. McCaustland, D.-P. Zheng, L.A. Hadley, G. Vaughn, S.M. Adams, T. Ando, R.I. Glass, S.S. Monroe, Use of TaqMan real-time reverse transcription-PCR for rapid detection, quantification, and typing of norovirus, J. Clin. Microbiol., 44 (2006) 1405–1412.

[50] X. Weng, S. Neethirajan, Aptamer-based fluorometric determination of norovirus using a paper-based microfluidic device, Microchimica Acta, 184 (2017) 4545–4552.

Table 1

Comparison of LOD with other NoV detection methods.

Detection method	Signal	Target	LOD	Reference
Microfluidic platform of aptasensor	Electrochemical	Virus RNA	100 pM	[46]
Photoelectro-chemical Biosensor	Electrochemical	Virus RNA	0.5 nM	[47]
RPzyme-integrated PCR	Colorimetric	Virus RNA	1 copy/ml	[48]
Nanozyme for visible detection	Colorimetric	NoV-LP	92.7 pg/ml	[31]
rRT-PCR (real-time RT-PCR)	PCR signal	Virus RNA	<10 copies/49 μl of reaction mixture (TaqMan)	[49]
Aptamer-based fluorometric determination	Fluorescence	NoV-LP	3.3–4.4 ng/ml	[50]
Bioluminescent enzyme immunoassay (BLEIA)	Luminescent	NoV capsid protein NoV	0.25 pg/ml 10^5–10^6 copies/g stool	[45]
LSPR-amplified MFIA	Fluorescence	NoV-LP Clinical NoV	0.48 pg/ml in feces 84 copy/ml in feces	This work

Legend for figures

Scheme 1. NoV detection scheme of LSPR-amplified MFIA.

Fig. 1. The nanoparticle image of TEM (A), SPIONs (B), AuNP/MNP composites (C) and confetto-shaped AuNP/MNP composites (D). Absorbance spectral analysis of AuNP/MNP composites and 11-MUA-capped AuNP/MNP composites (E). SQUID measurement of SPIONs (F) and AuNP/MNPs (G) with hysteresis curves.

Fig. 2. Effect of the morphology of nanomaterials on antibody conjugation and immunofluoro response. (A) ELISA result for antibody conjugation on nanomaterials. (B) Magnetofluorescence detection of NoV-LPs (10 pg/ml) using Ab-confetto-shaped and Ab-spherical AuNP/MNP composites.

Fig. 3. Fluorescence intensity scan results using a magnetic separation-based MFIA showed that fluorescence enhancement depends on the NoV-LP concentration (A) and the calibration curve (B). The confocal laser scanning microscopy image of the sandwich structure of NoV-LPs between Ab-QDs and Ab-AuNP/MNPs in a dark image (C), without laser scanning (D) and merged (E). Error bars in (B) indicate the standard deviation (n=3).

Fig. 4. NoV (genotype II.2,3 and 4) detection using clinical samples by LSPR-amplified MFIA (this work) (A) and by commercial ELISA kits (B). Error bars in (A) and (B) indicate the standard deviation (n=3).

Fig. 5. The selectivity test of the sensor. 5% BSA, human serum, 100 ng/ml of influenza virus A (H1N1, H9N2), 10^5 RNA copies/ml of zika virus and 100 ng/ml of hepatitis E virus-like particle (HEV-LPs) used as negative samples.

Takemura et al,, Scheme. 1

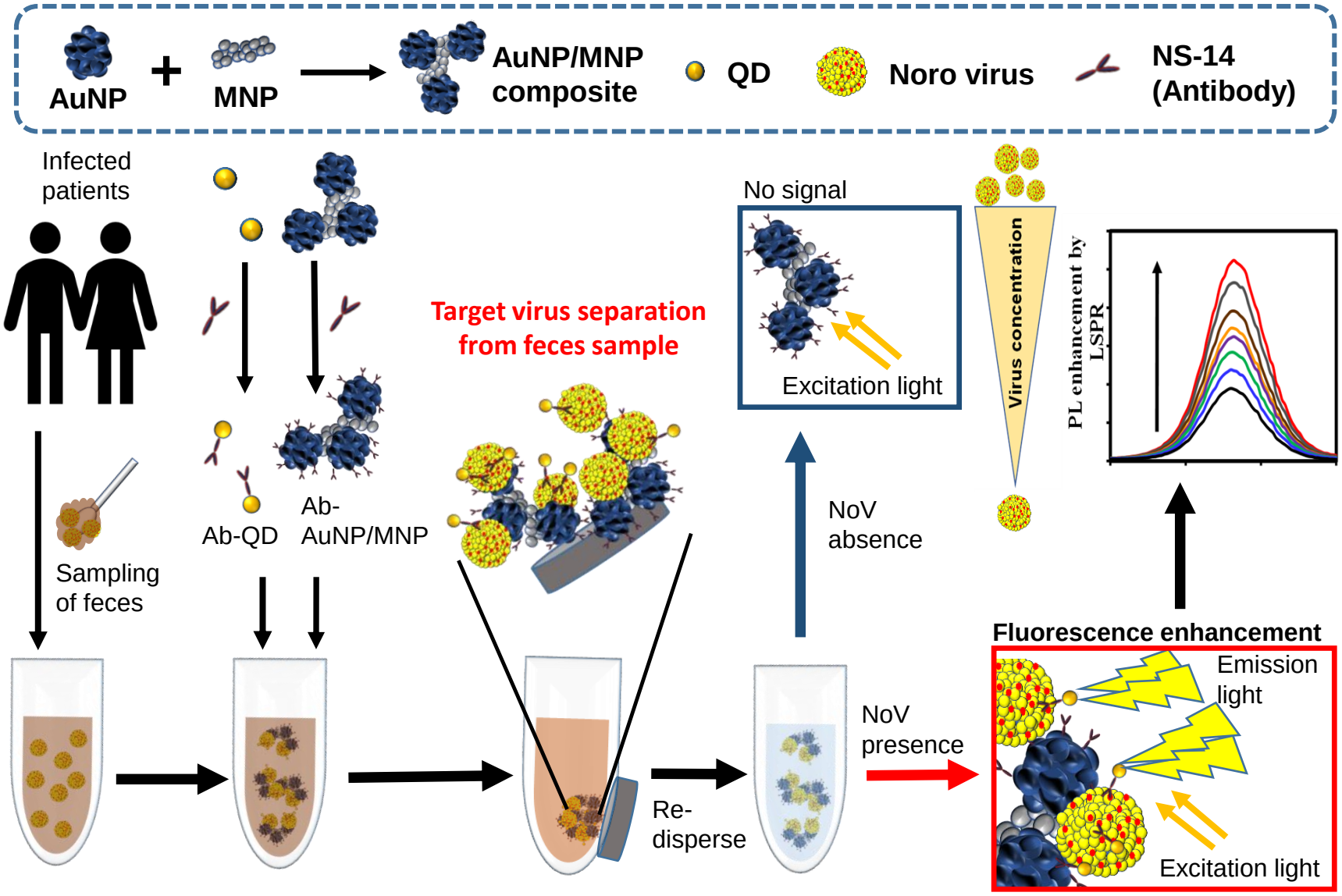

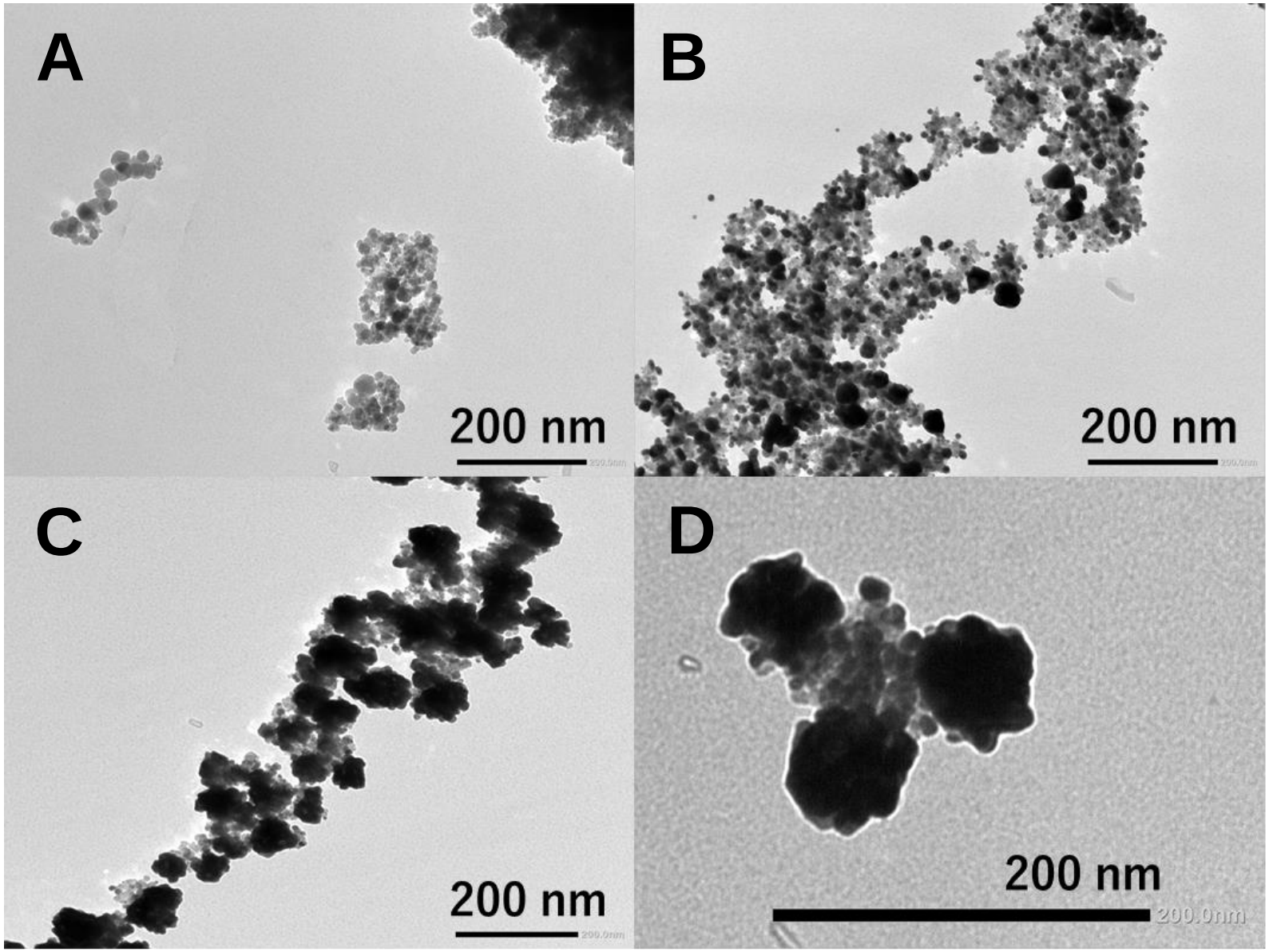
A
200 nm
B
200 nm
C
200 nm
D
200 nm
200.0nm

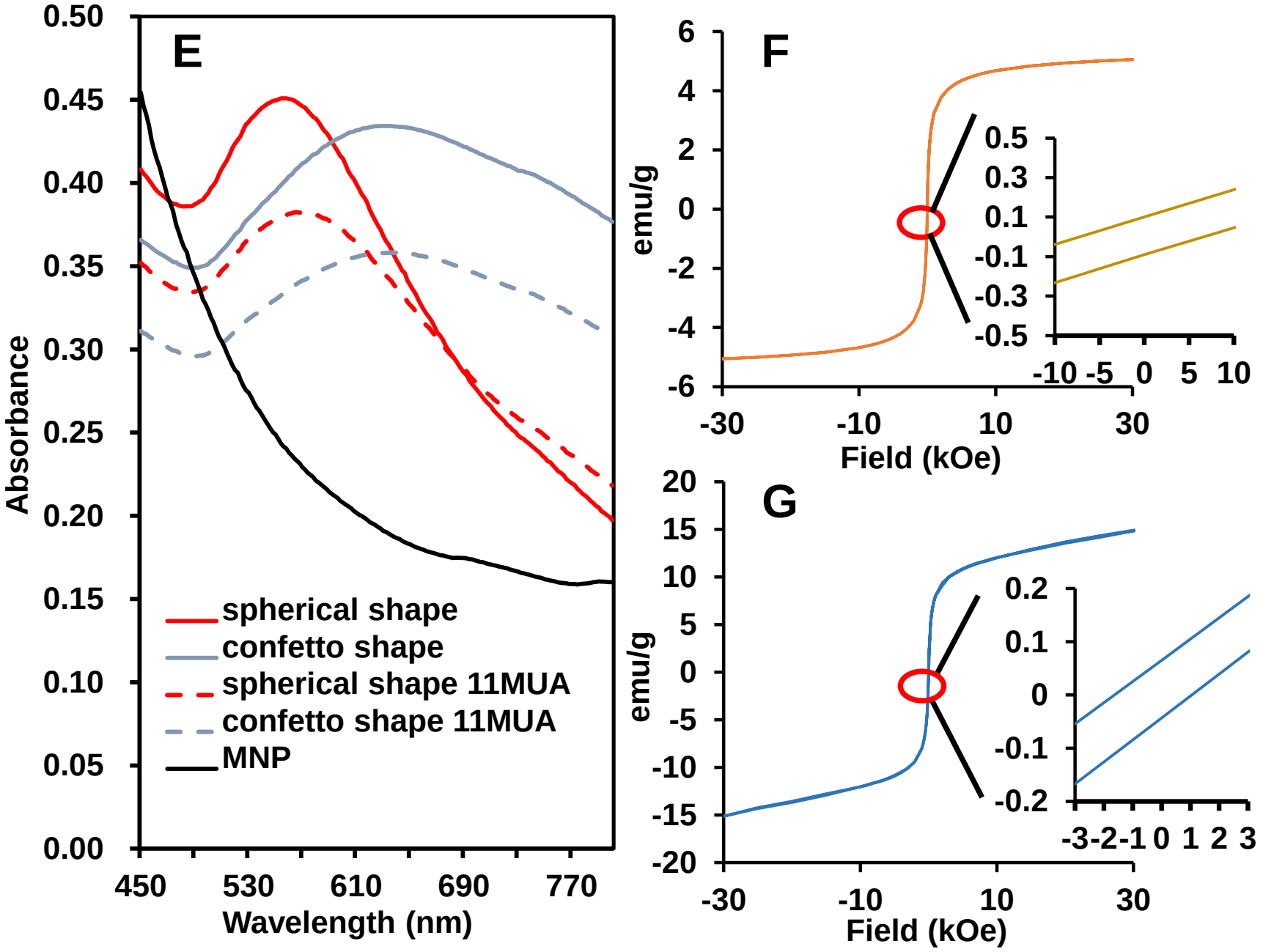
E
Absorbance
0.50
0.45
0.40
0.35
0.30
0.25
0.20
0.15
0.10
0.05
0.00
450
530
610
690
770
Wavelength (nm)
spherical shape
confetto shape
spherical shape 11MUA
confetto shape 11MUA
MNP
F
emu/g
6
4
2
0
-2
-4
-6
-30
-10
10
30
Field (kOe)
0.5
0.3
0.1
-0.1
-0.3
-0.5
-10 -5 0 5 10
G
emu/g
20
15
10
5
0
-5
-10
-15
-20
-30
-10
10
30
Field (kOe)
0.2
0.1
0
-0.1
-0.2
-3-2-1 0 1 2 3

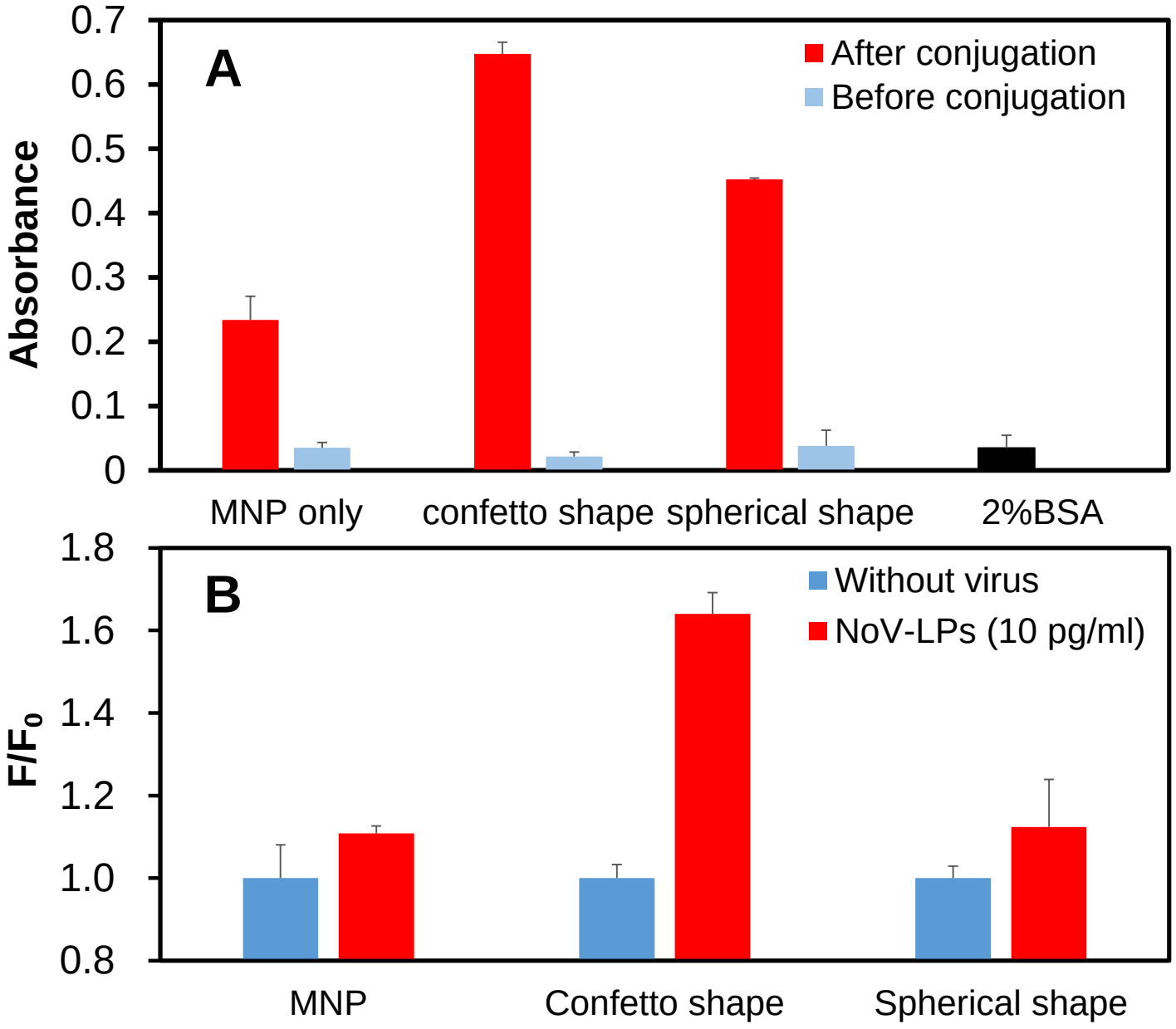
A
After conjugation
Before conjugation
Absorbance
0.7
0.6
0.5
0.4
0.3
0.2
0.1
0
MNP only
confetto shape
spherical shape
2%BSA
B
Without virus
NoV-LPs (10 pg/ml)
F/F0
1.8
1.6
1.4
1.2
1.0
0.8
MNP
Confetto shape
Spherical shape

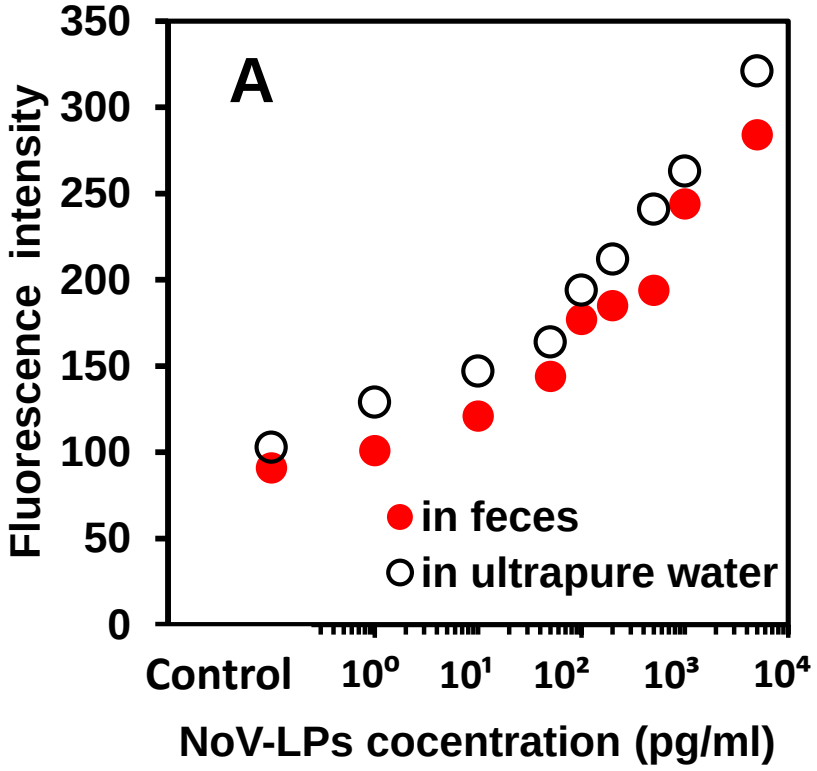
A
Fluorescence intensity
350
300
250
200
150
100
50
0
in feces
in ultrapure water
Control
10^0
10^1
10^2
10^3
10^4
NoV-LPs cocentration (pg/ml)

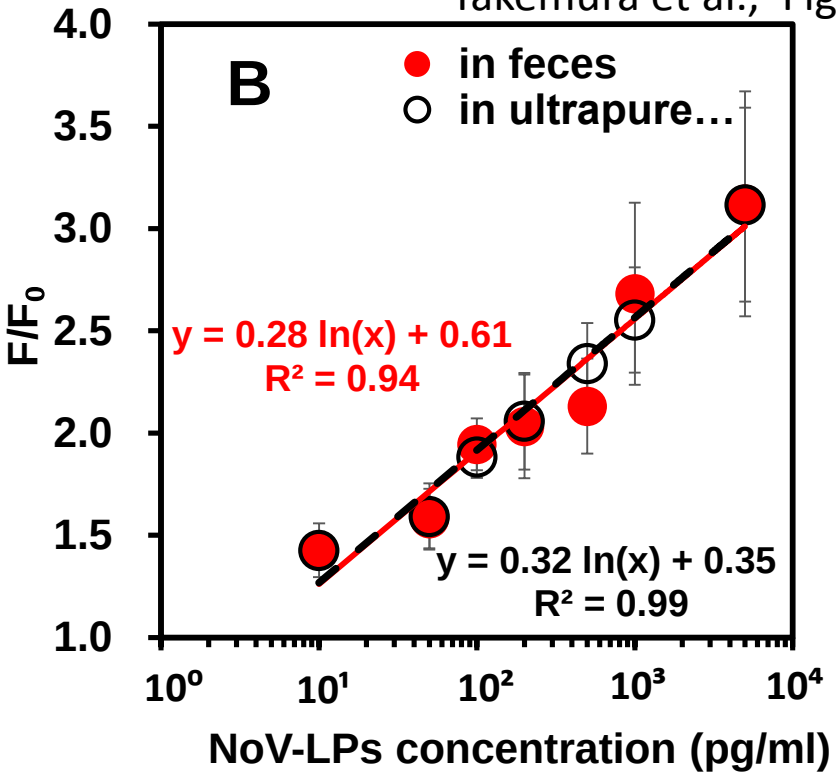
B
F/F_0
4.0
3.5
3.0
2.5
2.0
1.5
1.0
in feces
in ultrapure…
y = 0.28 ln(x) + 0.61
R^2 = 0.94
y = 0.32 ln(x) + 0.35
R^2 = 0.99
10^0
10^1
10^2
10^3
10^4
NoV-LPs concentration (pg/ml)

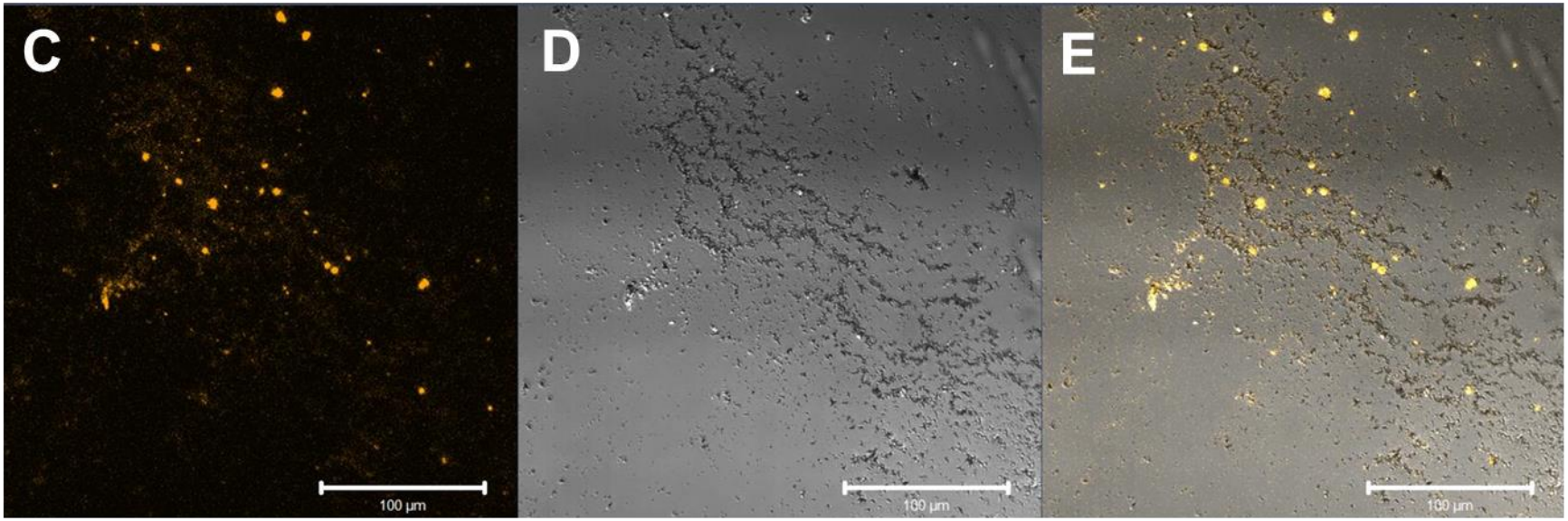
C
D
E
100 µm
100 µm
100 µm

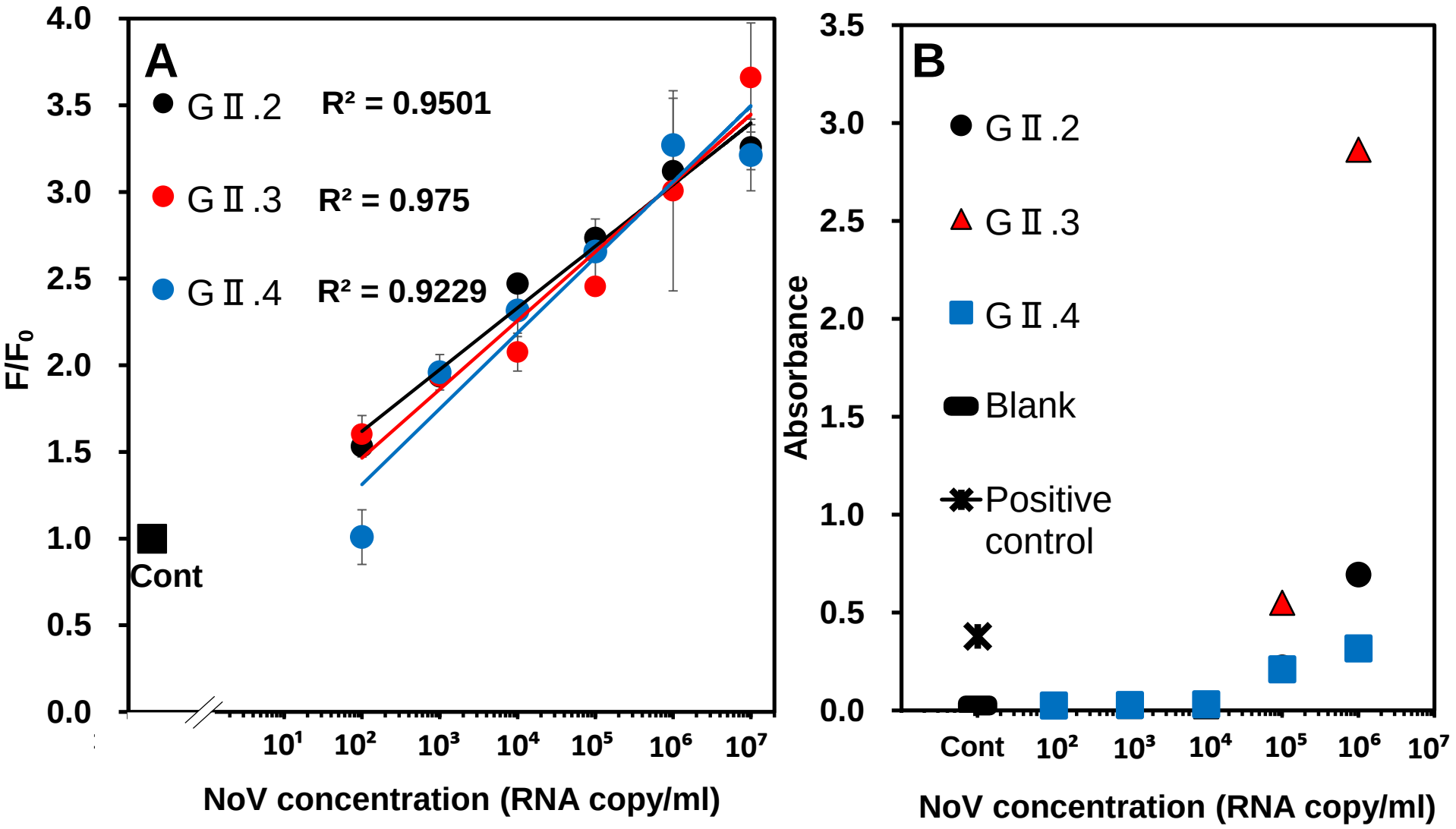
A
GⅡ.2
R² = 0.9501
GⅡ.3
R² = 0.975
GⅡ.4
R² = 0.9229
Cont
F/F0
4.0
3.5
3.0
2.5
2.0
1.5
1.0
0.5
0.0
10¹ 10² 10³ 10⁴ 10⁵ 10⁶ 10⁷
NoV concentration (RNA copy/ml)
B
GⅡ.2
GⅡ.3
GⅡ.4
Blank
Positive control
Absorbance
3.5
3.0
2.5
2.0
1.5
1.0
0.5
0.0
Cont 10² 10³ 10⁴ 10⁵ 10⁶ 10⁷
NoV concentration (RNA copy/ml)

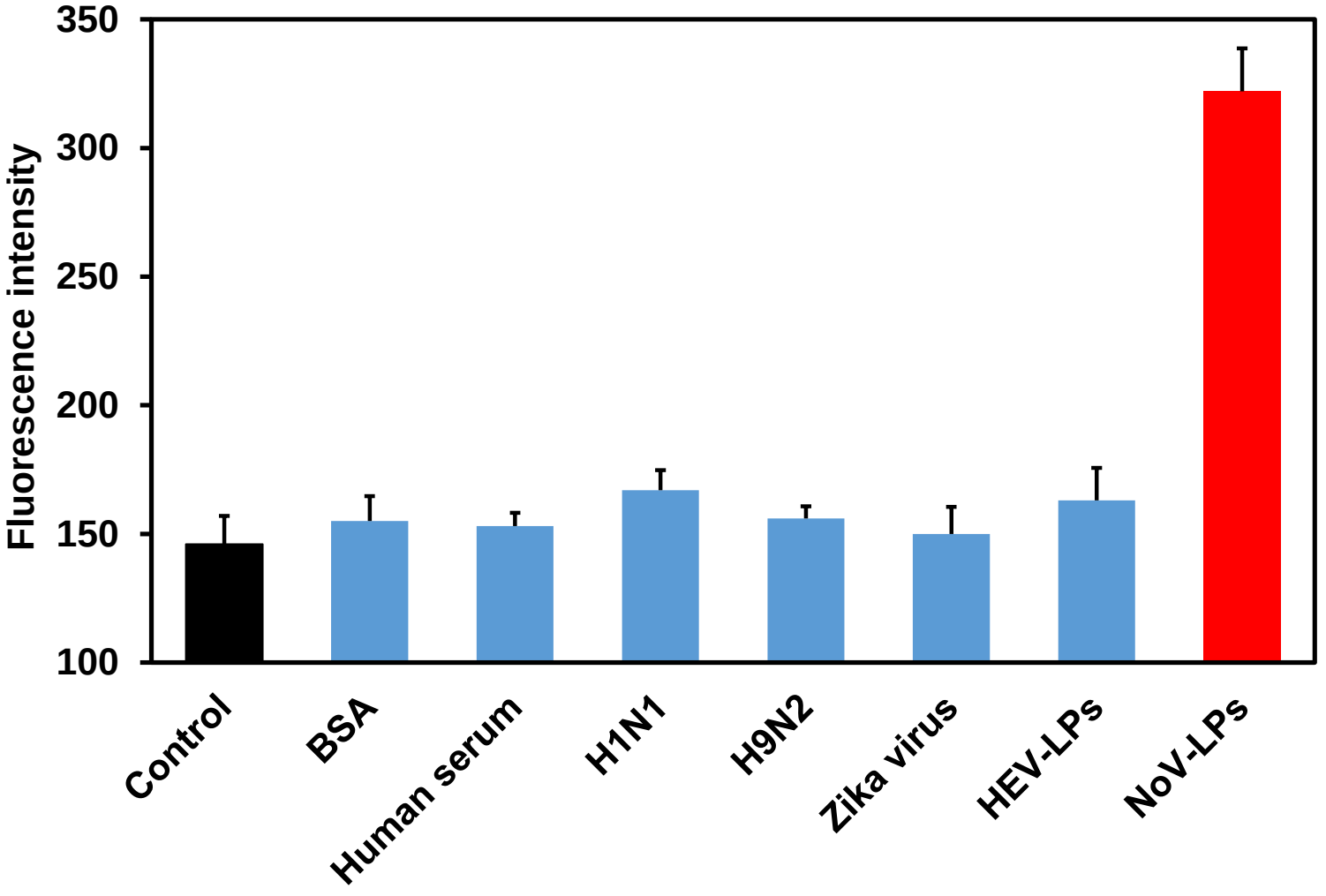
Fluorescence intensity
350
300
250
200
150
100
Control
BSA
Human serum
H1N1
H9N2
Zika virus
HEV-LPs
NoV-LPs

Supporting Information

Ultrasensitive detection of norovirus using a magnetofluoroimmunoassay based on synergic properties of gold/magnetic nanoparticle hybrid nanocomposites and quantum dots

Kenshin Takemura[a], Jaewook Lee[b,¶], Tetsuro Suzuki[c], Thoshimi Hara[d], Fuyuki Abe[d], Enoch Y. Park[a,b,*]

[a] Laboratory of Biotechnology, Department of Bioscience, Graduate School of Science and Technology, Shizuoka University, 836 Ohya, Suruga-ku, Shizuoka 422-8529, and [b]Research Institute of Green Science and Technology, Shizuoka University, 836 Ohya, Suruga-ku, Shizuoka 422-8529, Japan
[c]Department of Infectious Diseases, Hamamatsu University School of Medicine, 1-20-1 Higashi-ku, Handa-yama, Hamamatsu 431-3192, Japan
[d]Department of Microbiology, Shizuoka Institute of Environment and Hygiene, 4-27-2, Kita-ando, Aoi-ku, Shizuoka 420-8637, Japan

E-mail addresses:
takemura.kenshin.16@shizuoka.ac.jp (KT)
nanojaewook@outlook.com (JL)
tesuzuki@hama-med.ac.jp (TS)
toshimi1_hara@pref.shizuoka.lg.jp (TH)
fuyuki1_abe@pref.shizuoka.lg.jp (FA)
park.enoch@shizuoka.ac.jp (EYP)

[¶]Current affiliation: School of Materials Science, Japan Advanced Institute of Science and Technology, Asahidai 1-1, Nomishi, Ishikawa 923-1292, Japan
[*] Corresponding author.
E-mail address: park.enoch@shizuoka.ac.jp (E. Y. Park)

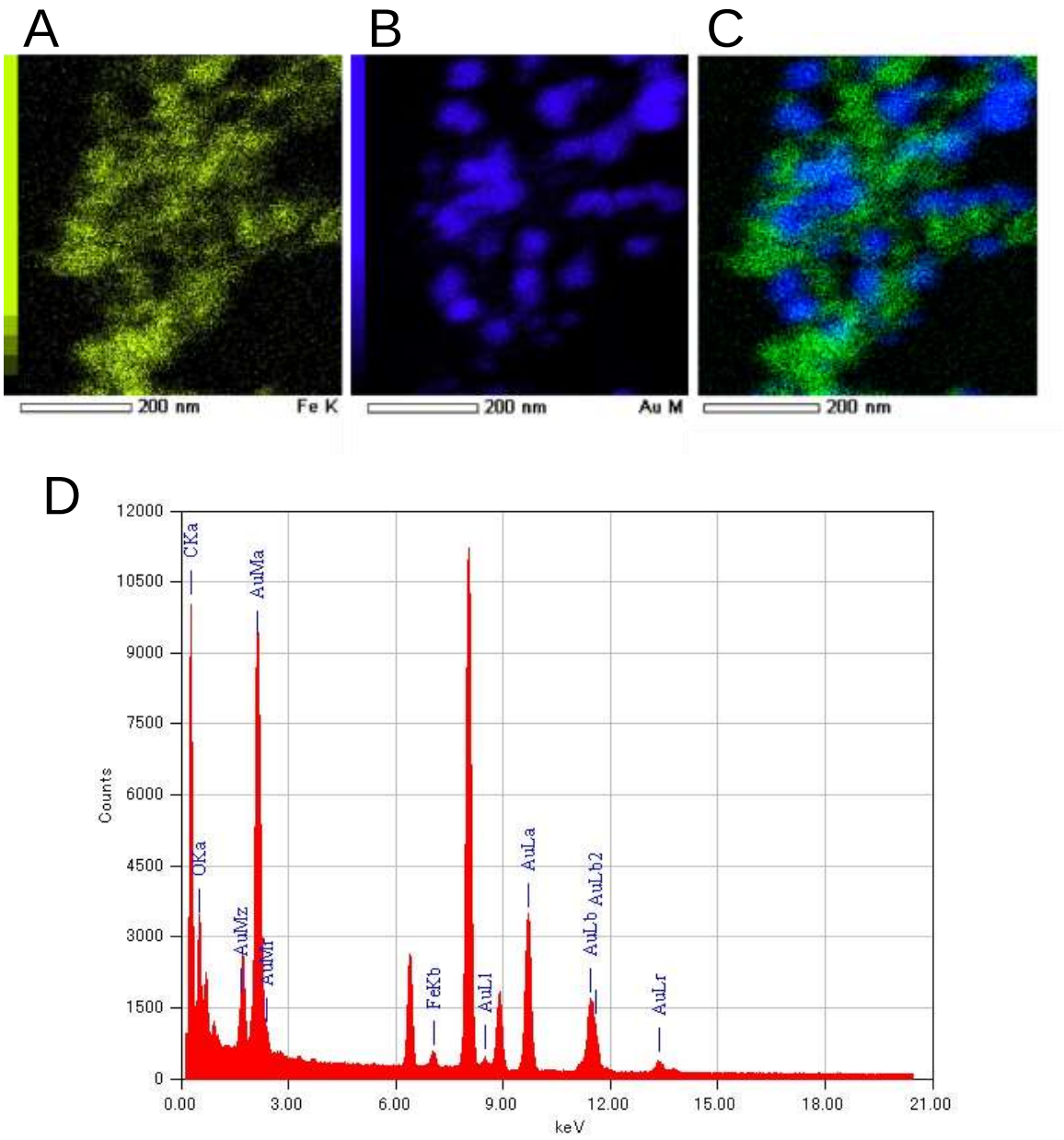

Fig. S1. A–C) Element mapping of AuNP/MNP composites (STEM). A) Fe mapping B) Au mapping and C) merged image of Au and Fe. D) The EDS analysis of 11-MUA-capped AuNP/MNP composite clearly show the peak of Au, Fe, C, and O.

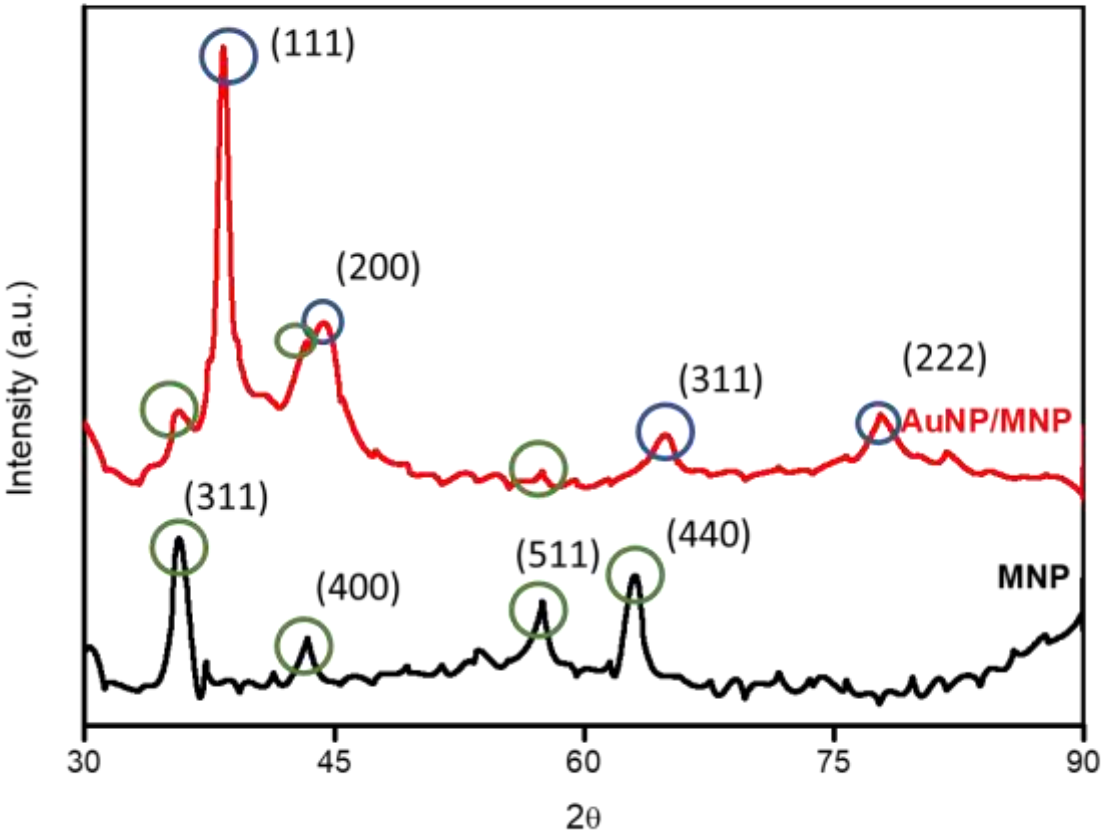

Fig. S2. X-ray powder diffraction patterns of AuNP/MNPs (—) and MNPs (—). Blue circle shows the peak of gold and Green circle shows the peak of MNP.

S3. Preparation of the norovirus solution

The conjugation of the anti-NS14 antibody to the QDs and AuNPs was confirmed using the ELISA. Briefly, 100 µl of conjugated Ab-QDs and Ab-AuNPs were added to separate wells of a 96-well polystyrene plate and incubated at 4 °C overnight. To confirm the specificity of the assay, 100 µl of 2% bovine serum albumin (BSA), as a negative control, was added to a separate well. After incubation overnight, the solution was washed three times using a solution of 200 µl PBS buffer containing 5% of Tween (PBST), and a blocking agent (10 µl of 5% skim milk) solution was added to each well and subsequently removed by washing three times with PBST. A dilution solution of 100 µl of anti-rabbit IgG-horseradish with 2% BSA (1:2000) was added to each well and incubated at room temperature for 1 h. A coloring chromogenic agent, 100 µl of TMBZ, was added to each well, which triggered a blue color as a confirmation of binding affinity between the Ab-QDs and Ab-AuNPs. The color of the solution changed from blue to yellow when the reaction was stopped with 50 µl of 10% H_2SO_4. The absorbance of the solution at 450 nm was measured using a microplate reader (Infinite® F500; TECAN) embedded with a reference filter at 655 nm.

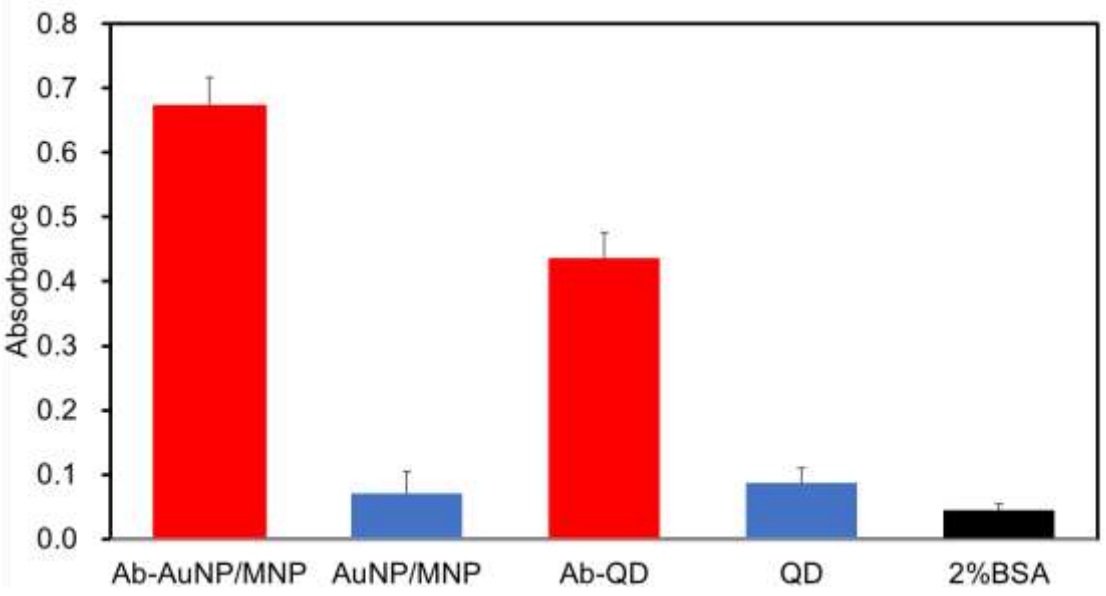

Fig. S3. Antibody conjugation of Ab-AuNP/MNP composites and Ab-QDs checked by simple ELISA. Red bar is Ab-NP and blue bar is before conjugation. 2%BSA used as a negative control (black bar).

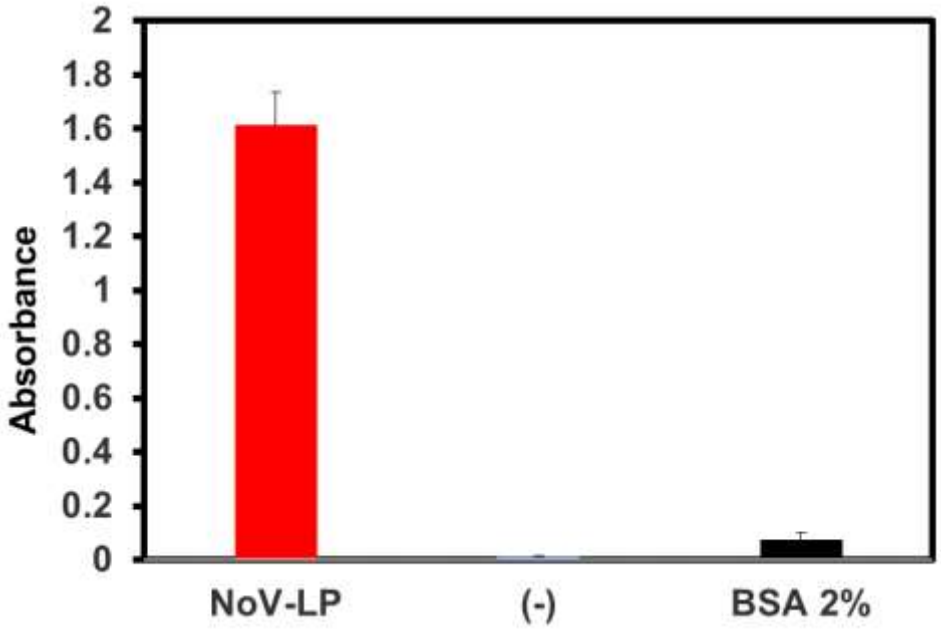

Fig. S4. ELISA results of anti NS14 antibody with NoV-LPs.

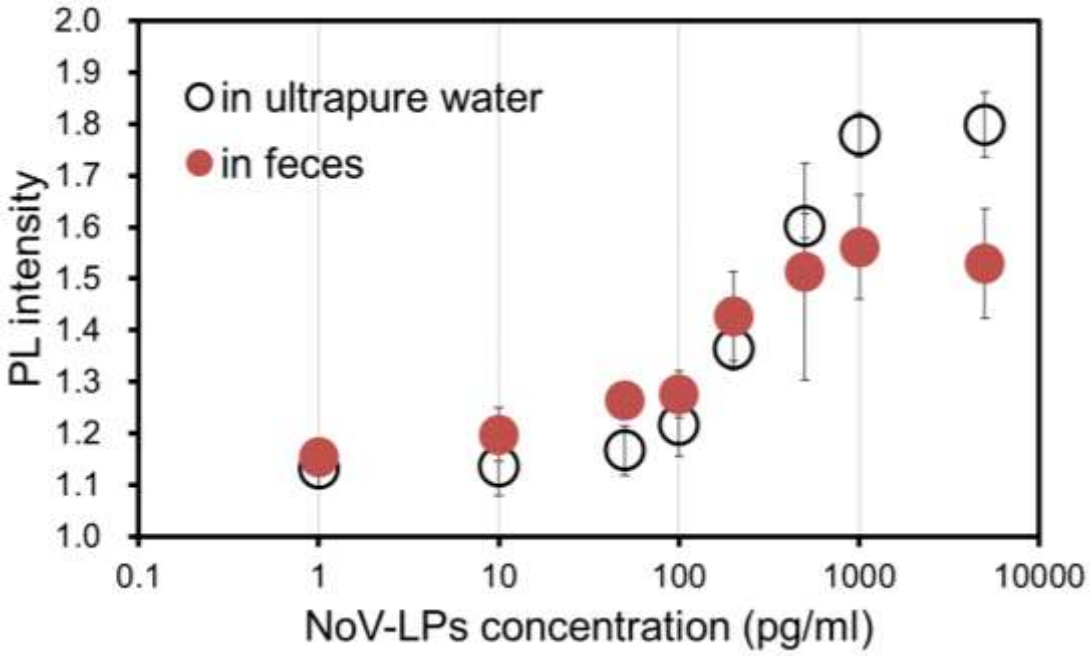

Fig. S5. Detection results using Ab-AuNPs and Ab-QDs in ultrapure water (○) and in human feces (0.1 mg/ml) (●).

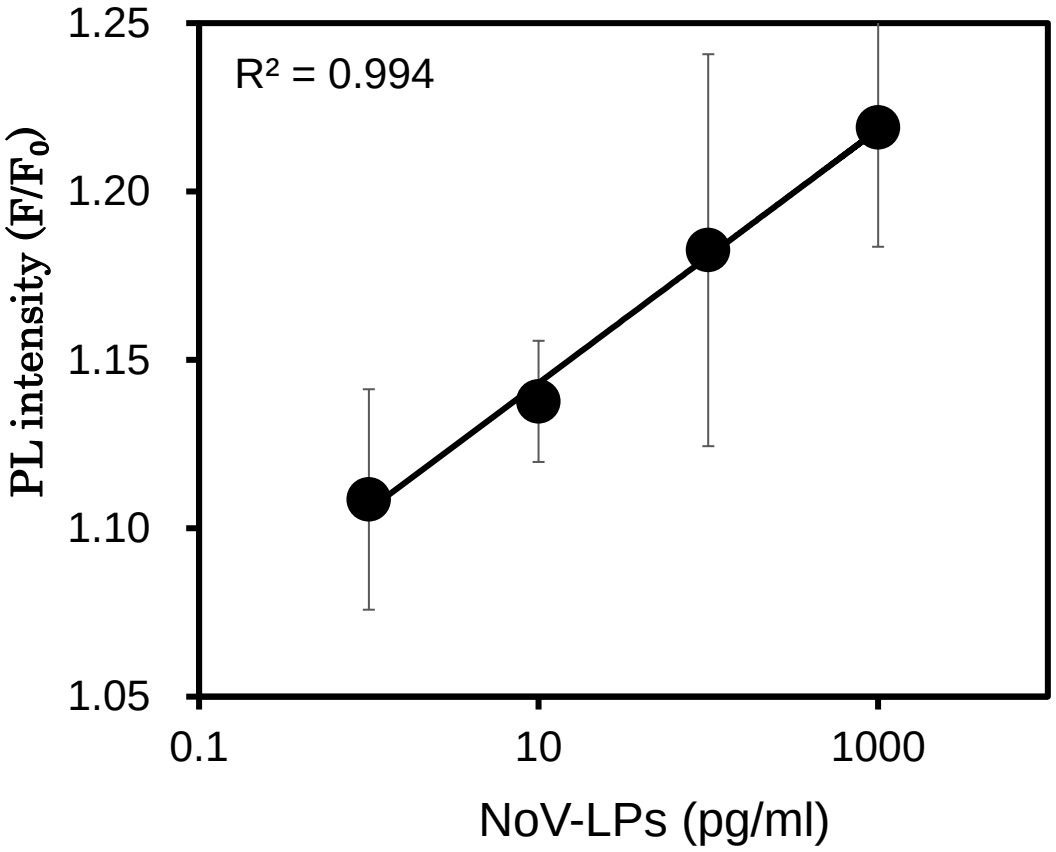

Fig. S6. Detection of fluorescence intensity using Ab-SPIONs and Ab-QDs without LSPR-amplifier. The fluorescence intensity increased depends on NoV-LPs concentration.